Composite Structures 139 (2016) 199–209

Contents lists available at ScienceDirect

Composite Structures

journal homepage: www.elsevier.com/locate/compstruct

Investigation on the structural behavior of a metallically 3D-reinforced CFRP/CFRP joint using a variable search based on finite element analyzes

Holger Lang [a,*], Ana Carolina Nogueira [a], Michael Jürgens [b], Elke Hombergsmeier [b], Roland Hinterhölzl [c], Klaus Drechsler [c]

[a] Fraunhofer Institute for Chemical Technology, Branch Functional Lightweight Design FIL, Am Technologiezentrum 2, 86159 Augsburg, Germany
[b] Airbus Group Innovations, P.O. Box 800465, 81663 Munich, Germany
[c] Technische Universität München, Institute for Carbon Composites, Boltzmannstraße 15, 85748 Garching, Germany

ARTICLE INFO

Article history:
Available online 8 December 2015

Keywords:
Joining technique
Pinning
Reinforcement
Simulation
Hybrid structure
Design of experiments

ABSTRACT

A numerical study on the structural mechanics of bonded composite structures, which were interlaminary reinforced by metallic sheet and pin elements, is presented in this paper. For the investigation of the potential of this reinforcing technology, finite element models on meso and macro scale were studied, which were successfully validated against experimental test results. On the example of quasi-statically loaded single-lap shear test specimens, the macro scale model was used to implement different configurations of the reinforcements including variations of the pin geometry as well as their arrangements. Passing a variable search according to Shainin, the influences of various design factors on the structural performance of the reinforced joints were evaluated. In addition, the main effects were identified as the pin and sheet thickness among others concerning the applicable load as well as the elongation of the joint. Furthermore, the analyzes of the interdependencies showed, that the majority of the variables weakens the effects of the other ones.

1. Introduction

In recent years, the mass share of carbon fiber reinforced plastics (CFRPs) in important structural aerospace components has been increased significantly, which is demonstrated by the Airbus A350XWB or the Boeing 787 Dreamliner. In the automotive industries, composites played a rather subordinate role in case of primary structures of cars produced in large quantities. This fact was essentially changed with the market introduction of BMW's i-series. As a result from the rising importance of composite materials, the need for appropriate joining techniques has been emerging. These are necessary to realize structures, which can take advantage of the whole lightweight potential of CFRP and fulfill the demand of structural integrity.

Adhesively bonding would meet those requirements, however, is suffering on unsatisfactory damage tolerance in case of failure. As a consequence, certification of this joining technique for the application at primary aircraft structures implies the request of a secondary load path. In practice, these requirements are satisfied by the supplementary usage of state-of-the-art joining techniques as bolts or rivets, as it is described by Camanho and Hallet [1], despite of their detrimental influence on the structural mechanics of the FRP material. These drawbacks are primarily caused by drilling holes, which are necessary to affix the reinforcements. By those, the load-carrying fiber structure is cut, which leads to stress concentrations around the holes, as the load is bypassed to the fibers located nearby. These regions are often identified as the weak areas in the joined structure as described by Grüber et al. [2]. As consequence, the design of such fail-safe structures leads to an additional introduction of mass by the own weight of the metallic elements and, in addition, by the obligatory enhancement of the composite cross-section to meet the requirements.

Focus of the presented task was the investigation of a novel joining method based on the reinforcement of bonding between two composite parts, whose capability was proven by Nogueira et al. [3]. The covered interlocking is created on meso scale by the implementation of three-dimensionally formed metal inserts, which avoids the disadvantages of conventional form closure techniques described above. The structural performance was numerically analyzed on single-lap shear geometries featuring a combination of shear and peel stresses in the run-out areas.

* Corresponding author.
E-mail addresses: lang_holger@t-online.de (H. Lang), michael.m.juergens@airbus.com (M. Jürgens), elke.hombergsmeier@airbus.com (E. Hombergsmeier), hinterhoelzl@lcc.mw.tum.de (R. Hinterhölzl), drechsler@lcc.mw.tum.de (K. Drechsler).

http://dx.doi.org/10.1016/j.compstruct.2015.11.040
0263-8223/

For the analysis of the structural mechanics a detailed finite element (FE) model according to the methods discussed by Lang et al. [4] was implemented in *ABAQUS*. Due to the high effort concerning model implementation and calculation time, a simplified finite element model on the basis of a multi scale approach was developed for the extensive parametric studies. Complementary to the numerical work, experimental tests were performed in order to validate the numerical implementation.

The validated implementation method was used to evaluate the responsible design variables of this reinforcing method concerning the applicable load and the corresponding elongation with a variable search according to Shainin et al. [5,6]. The sheet and pin thickness, the design of the stamped areas as well as the distribution of the pins were identified as the most influential parameters.

The investigation of the interdependencies between the most important design variables showed a varied behavior concerning the two objectives. Especially regarding the elongation of the joint, this analysis showed a weakening of several variables' effects among each other, which was caused by the interdependencies.

2. Reinforcing concept and its manufacturing

The approach of reinforcing, which is dealt with in this study, focuses on the generation of interlocking by weakening the composite material as low as possible. In contrast to state-of-the-art form closing methods, the presented reinforcing technique creates an interlocking on such a small scale, that the fibers are deflected around the pins during the implementation, which enables the preservation of the fibers in general at a high grade. In a particular way, the presented concept picks up methods of reinforcing joints between composite parts by integrating elements in z-direction in order to enhance the structural performance. Classical z-pinning is predicated on the implementation of carbon rods in z-direction as reviewed by Tao et al. [7]. Mouritz [8], Rugg et al. [9] and Byrd and Birman [10] evaluated it as a promising method to reach essential improvements of the mechanical performance. Different research groups as Kolesnikov et al. [11] and Karpov [12] described the application of metal pins including a plastic deformation capability as reinforcing elements, which proved to be beneficial considering energy absorption. In addition, the potential of this reinforcing method under conditions determined by higher ambient temperature and humidity was discussed by Son et al. [13].

A method of the creation of cylindrical reinforcing elements by welding them on a metallic substrate is described by Ucsnik et al. [14]. Through a variation of the process parameters the pin geometry including the one of the head can be affected. By the usage of this reinforcing method at hybrid double-lap shear test specimens, the sustainable load could be increased as well as the damage tolerance. The application of these reinforcements at composite to composite joints is proven by Ucsnik and Staffenberger [15]. A metal sheet containing welded reinforcements on both sides was integrated into the composite structure before the curing process. As result, a significant improvement of the energy absorption could be registered, but a decrease of the initial stiffness compared to referential co-bonded unreinforced single-lap shear test specimens was observed, too. A technique of creating three-dimensional reinforcements on a metallic sub-structure by additive layer manufacturing is the focus of the research work done by Bianchi [16]. Based on the used method, different metallic materials can be used to create pins of various geometries. Under different loading conditions, improvements of the structural performance could be reached concerning the hybrid connection of metal to composite material.

The method focused within this paper is concentrating on the reinforcement of the bonding between two composite structures. The concept is based on the integration of thin metallic reinforcing structures, that are produced by a cost and time saving manufacturing process. In addition, the method of metallic inserts enables the precise positioning of the reinforcements within the overlap area. Thin plane metal foils were stamped showing the later design of the reinforcements (Fig. 1(a)). Afterwards, the reinforcing pins are bent into a ninety degrees angle alternately upwards and downwards (Fig. 1(b)) using a specially designed bending tool of Hölzl Stanz- und Feinwerktechnik. The bending also considers the springback effect described by Groze et al. [17], which results in a practical bending angle greater than ninety degrees. The so created reinforcement sheet is integrated into the CFRP–CFRP joint using a co-curing process. The metal insert is joint with the first uncured composite part, which consist of prepreg material, before the first curing cycle.

During the curing under pressure and temperature in an autoclave, the resin of the preimpregnated composite material establishes a bonded connection between the composite and the metal reinforcement (Fig. 2(a)). The cured CFRP adherend already including the reinforcement is joint to the remaining uncured composite part in the second curing cycle adding an adhesive film (Fig. 2(b)). During this curing step, the areas between the metallic fillets of the metal insert are filled with epoxy material from the prepreg as well as the adhesive. The parameters of these autoclave cycles are schematically presented in Fig. 3. The essential part is set by an additional holding zone during the application of the temperature, which generates a viscous state of the resin, that the implementation of the pins into the composite material is improved. As analyzed by Nogueira [18], too, a negative influence on the structural mechanics of the prepreg material was not observed.

3. Test specimens and experiments

Considering the analyzes of the structural mechanics of the reinforcing concept, single-lap shear geometries were selected, as these provide realistic loading conditions of a combination of shear forces within the overlap as well as peeling stresses especially in the run-out areas, as they appear in real life applications as e.g. stringer-skin run-outs of an aircraft fuselage. Among other things for the validation of the finite element models, these geometries were experimentally tested. Within the presented work, two different geometries were made used of.

Concerning the comparison to the finite element model on macro scale, single-lap shear test specimens with dimensions according to ASTM 5868 standard [19] were used, see Fig. 4. The CFRP adherends of all test specimens consisted of the unidirectional aerospace prepreg material HexPly® M21/T800S from Hexcel [20]. Their stacking of $[-45^\circ/45^\circ/0^\circ/90^\circ/0^\circ]_s$ implicated an overall thickness of $t = 1.93$ mm per component. The reinforcements were produced out of stainless steel 1.4301 of a thickness from $t = 0.2$ mm to $t = 0.4$ mm. As film adhesive, which creates the connection within the second curing cycle between the already cured and the uncured part, FM®300K with a thickness of $t = 0.013$ mm produced by Cytec Industries was used.

Regarding the validation with the detailed finite element model, a single-lap shear test specimen with reduced dimensions in contrast to ASTM 5868 [19] was used, cf. Fig. 5, in order to reduce the modeling and computational effort.

During the second curing step, certain regions of the cured assembly exhibit resin pockets especially in the spaces between the metallic fillets of the inserts. The predominant material over there is seen as a mixture of FM®300K and HexPly® M21 resin.

For the validation of the developed numerical implementation, different configurations of reinforced single-lap shear specimens were experimentally tested. The manufacturing process of the

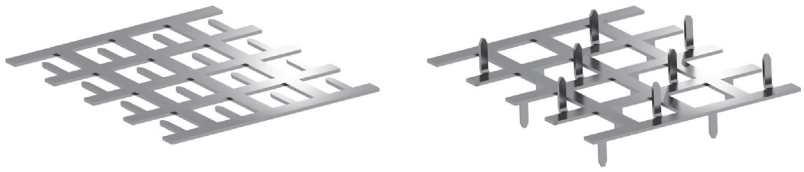

(a) Stamping (b) Bending

Fig. 1. Manufacturing process of the reinforcing inserts.

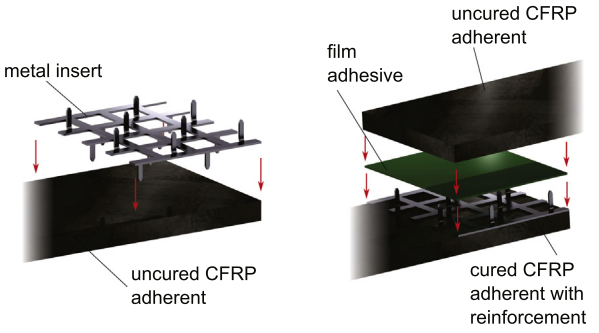

(a) First curing cycle (b) Second curing cycle

Fig. 2. Co-curing joining process of the reinforced joint.

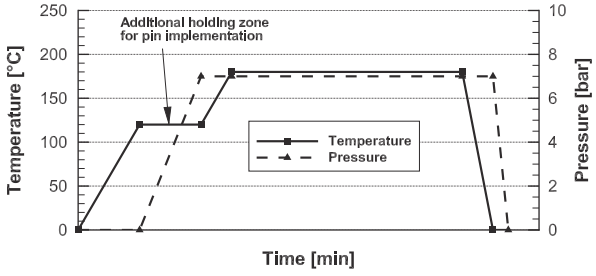

Fig. 3. Schematic of the parameters of the autoclave curing cycle.

specimens was performed according to the description above. The tensile tests were conducted on a Zwick Z250 tensile test machine with a load range of up to 250 kN. The specimen loading rate was set to 13 mm/min. Besides the crosshead travel the local elongation around the reinforced overlap area was determined by an 80 mm extensometer considering the specimens of reduced dimensions and a 50 mm extensometer at the specimens according to ASTM 5868. The output of the extensometers were used for the comparison against the numerical results.

4. Finite element modeling of reinforced joints

Within this task numerical modelings of the reinforcing technique on two levels of detail were realized. The finite element models were created and calculated in the commercial software *ABAQUS/explicit* 6.14. The implementation strategy was aligned to a multi scale approach.

4.1. Set-up of the detailed numerical model

A detailed finite element model of the reinforced single-lap shear test specimen with the reduced dimensions showed in Fig. 5 was implemented using the procedures described by Lang et al. [4]. The global set-up of the detailed numerical model including the assignment of specific materials and interfaces is constituted in Fig. 6.

The CFRP components were modeled using *ABAQUS* C3D8 elements, which feature a complete three-dimensional stress state. The necessary material data were taken from the work of Ilyas [21]. Considering the anisotropy of the layered composite structure, local orientations were applied. The corresponding material model was realized by an anisotropic elastic behavior. The failure mechanism and subsequent degradation were assigned using a custom *VUMAT* user subroutine [22] to include Puck's failure criterion [23] into the analysis. The three-dimensional formulation of the criterion was implemented according to the recommendations by Deuschle [24] and Puck and Deuschle [25]. The stainless steel 1.4301, which the metal insert consisted of, was implemented using an elastic behavior followed by a plastic hardening defined by tabular input. The fracture was realized by allocating a ductile failure criterion including a linear degradation. The underlying characteristics of the metal deformation were gained from experimental tensile tests. The epoxy based material between the metallic fillets was implemented using a linear-elastic approach by making use of the data taken from the research work of Joudon et al. [26]. The boundary conditions were applied on the edges of the CFRP adherends at a distance around the joint representing the experimentally measured distances of 80 mm. These nodes were coupled to reference points, to which the particular boundary conditions were assigned. On one site, all the translational degrees

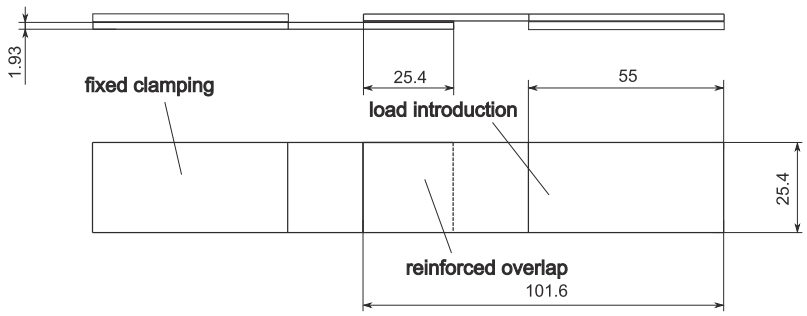

Fig. 4. Geometry of single-lap shear specimens according to ASTM 5868 standard.

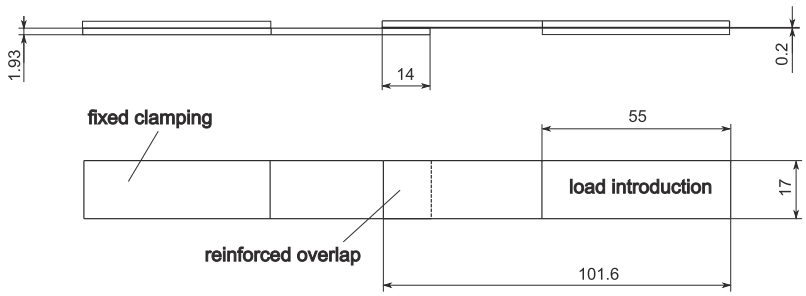

Fig. 5. Geometry of the single-lap shear specimen with reduced dimensions.

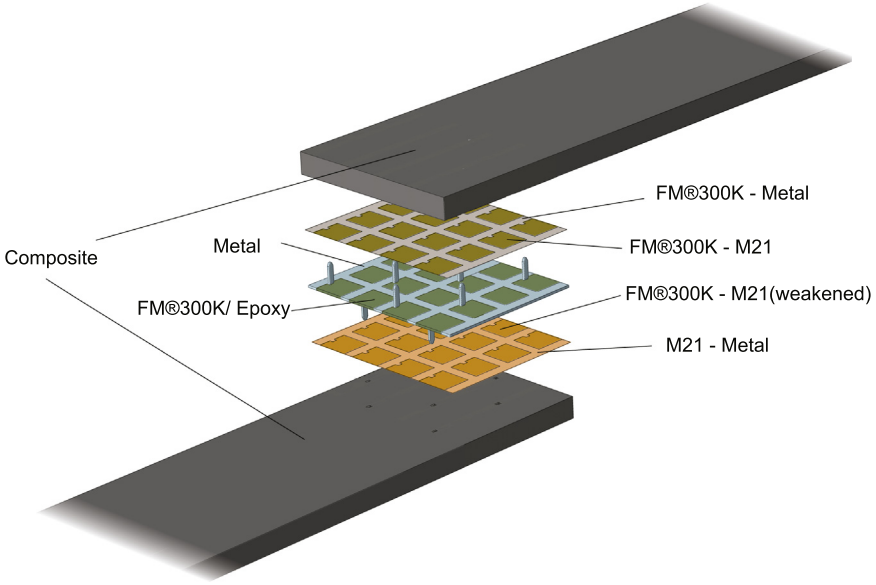

Fig. 6. Schematic of the FE implementation and relating material assignment.

of freedom were blocked, on the other site a linear increasing displacement in loading direction was applied by locking the other variances.

4.2. Interface implementation by cohesive zones

The links between the different materials including an optional failure mechanism were realized by cohesive zones. As a result from the co-curing joining process, different material combinations were responsible for the bonding characteristics between the metal and composite. The bonding connections emerging from the first joining step as well as the connection between the reinforcing elements and the surrounding composite material are merely influenced by the resin of the prepreg material. During the second joining step the connection is mostly initialized by the additionally applied FM®300K adhesive film. The cohesive characteristics between the composite materials and the epoxy filled areas were calibrated by taking into account experimental results of bonded CFRP–CFRP test specimens and were implemented according to the results described by Lang et al. [27]. The cohesive zones were modeled using a bilinear traction-separation law as described by Lang et al. [4] regarding *opening* and *shear* failure modes. The particular energy release rates G_c were taken from the work of Bianchi [16] and Camanho et al. [1]. The initial stiffness K was calculated according to (1), see the recommendations of Dassault [28]:

$$K = \frac{\alpha \cdot E}{h} T_0 \tag{1}$$

The coefficient α was set to $\alpha = 50$ as proposed by Turon et al. [29]. E represents the young's modulus of the surrounding material and h the thickness of the adherents. T_0 was defined as $T_0 = 1.0$ as proposed by Dassault [28]. The toughness s of the bilinear approach was used for calibrating the behavior against experimental data.

Table 1 summarizes the data of the essential interfaces between metal and the prepreg material HexPly® M21/T800S and the Cytec FM®300K adhesive film used alongside the epoxy filled areas. The

Table 1
Calibrated material data of the cohesive zones.

metal-CFRP		
Normal stiffness K_n	[kN/mm³]	259
Shear stiffness $K_s = K_t$	[kN/mm³]	130
Normal toughness s_n^0	[MPa]	40
Shear toughness $s_s^0 = s_t^0$	[MPa]	40
Energy rel. rate (normal) G_{Ic}	[N/mm]	0.20
Energy rel. rate (shear) $G_{IIc} = G_{IIIc}$	[N/mm]	0.550
CFRP-Cytec FM®300K-CFRP		
Normal stiffness K_n	[kN/mm³]	259
Shear stiffness $K_s = K_t$	[kN/mm³]	130
Normal toughness s_n^0	[MPa]	55
Shear toughness $s_s^0 = s_t^0$	[MPa]	54
Energy rel. rate (normal) G_{Ic}	[N/mm]	1.3
Energy rel. rate (shear) $G_{IIc} = G_{IIIc}$	[N/mm]	2.02

energy release rates at those cohesive zones modeling the FM®300K connection with the metallic insert were calibrated using double cantilever beam tests relating to this material combination, to include eventually occurring thermal effects and the weakening due to the reduced adhesion to the metallic substrate. Compared to the CFRP–CFRP bonding, the energy release rate was weakened by about 30%, which shows a similar magnitude as presented by Yan et al. [30].

4.3. Validation of the detailed numerical implementation

Fig. 7 includes the load–elongation curves covering the cutout of 80 mm around the joint generated by experimental tests as well as the numerical solution.

Considering the initial stiffness, which is basically induced by the properties of the adherends, the conformity of the experimental gained data with the numerical solution was proven. The point of first failure, which is merely caused by a fracture of the bonding at the edges, was observed between $f = 2700$ N and $f = 2900$ N at the experiments. The numerical results matched this range by an initial failure of the bonding surface at $f = 2750$ N.

The structural characteristics between the initial and final failure are mainly influenced by the reinforcement and the metallic insert. The experiments showed a visible stiffness reduction leading to an ultimate load of $f = 3150$ N to $f = 3600$ N. The point of final failure was reached by an elongation between $e = 0.19$ mm and $e = 0.20$ mm. The overall characteristics were reproduced by the numerical modeling. The maximum applicable load was amounted to $f = 3600$ N, which represented the upper limit of the experimental data. The point of final failure was coupled to an elongation of $e = 0.19$ mm, that is in the range of the corresponding experimental values. It could be summarized, that the detailed numerical implementation was able to reproduce the characteristics of the experimental tests and generated results, which are located within the range of the experimental curves.

4.4. Simplified finite element model

Due to the high effort concerning modeling as well as calculation time, the detailed implementation method was just reasonable considering the implementation of small overlapping areas with a comparatively low number of reinforcements. For the implementation of single-lap shear test specimens according to ASTM standard 5868 [19] providing an increased number of pins, a simplified implementation method was developed, see Fig. 8.

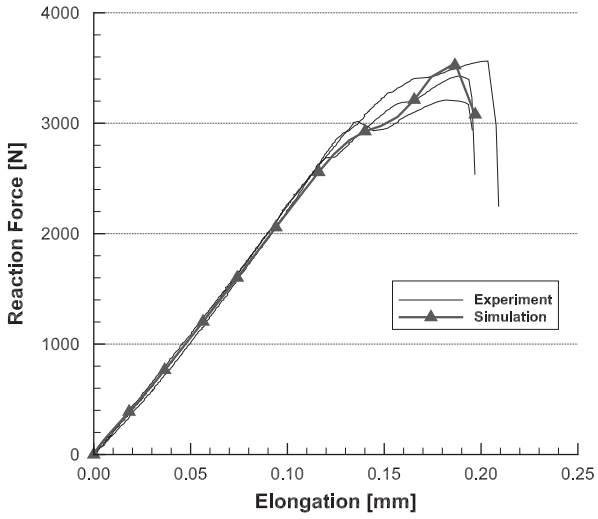

Fig. 7. Comparison between experimental and numerical results of a single-lap shear test specimen.

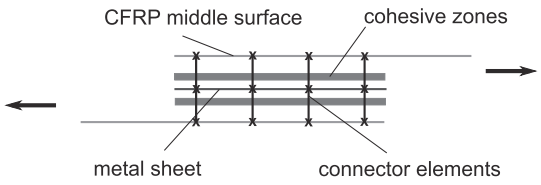

Fig. 8. Schematic of the simplified model of the reinforced joint.

The thin-walled structures of the CFRP adherends, the metallic insert as well as the epoxy filled areas were modeled with two-dimensional shell elements of *ABAQUS* type S4R. They were assigned an average element size of 1.2 mm concerning the composite adherends and 0.5 mm regarding the two last named ones to fulfill the requirements concerning ratio of applied thickness to width, which follows from the assumption of thin-walled structures.

The elements of the CFRP structure contained a layered section behavior to reproduce the stacking of the composite material. In contrast to the detailed implementation, the simplified model did not respect the holes created by the reinforcing elements. Hence, the ideally considered composite material was weakened according to the methods described by Lang et al. [27]. The elements of the metallic inlet and the epoxy zones included a homogeneous section assignment with isotropic material properties. The connections between the individual parts were modeled using cohesive zones as it was done in the detailed implementation, too. They featured an average element size of 0.2 mm.

The reinforcing pins themselves were simplified using a multi-scale-approach. The detailed implementation of the pin including the bonding characteristics to the surrounding composite material was replaced by connector elements of *ABAQUS* type CONN3D2, cf. Fig. 9, which state a connection between two nodes: one of the composite and one of the metal insert, which corresponds to the position of the reinforcing pin. Each element contains three rotational and translational degrees of freedom each. Whereas the rotational degrees of freedom were set to rigid, the translational ones were assigned structural mechanics according to the main load cases considering the relative motion from the metal reinforcement to the composite material. The underlying load–displacement curves were gained from single-pin simulations, cf. Fig. 10.

The corresponding finite element model included a cutout of the detailed numerical model with edges chosen at such a distance, that boundary effects on the structural mechanics of the reinforcement were negligible. The linear increasing displacement of the pin was applied to a reference point, which was coupled to the root of the reinforcement. The main load cases of the analyzed test specimens were identified to normal loading in z-direction and shear resulting from a motion of the pin root in x-direction, cf. Fig. 11.

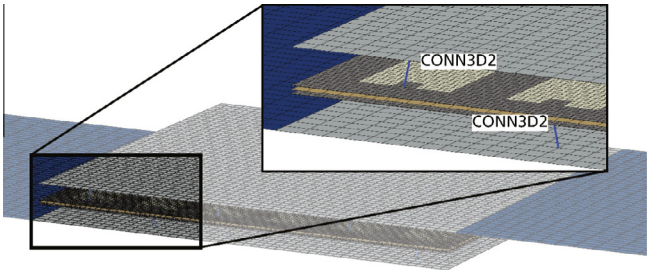

Fig. 9. Simplified finite element model of a reinforced single-lap shear test specimen.

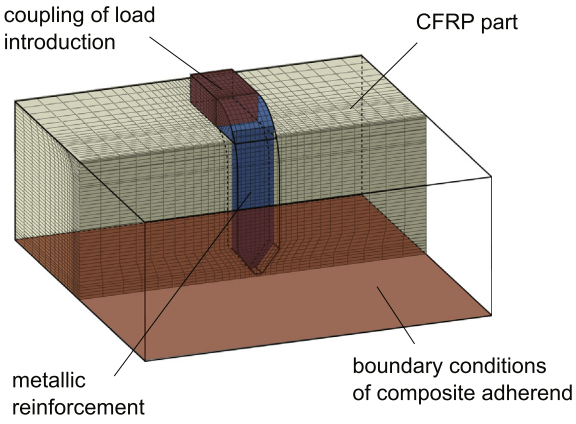

Fig. 10. Finite element model of a single-pin simulation.

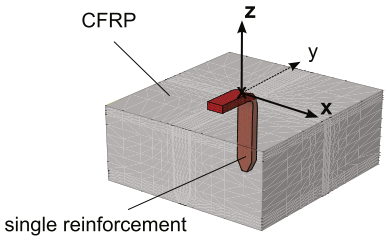

Fig. 11. Schematic of a single-pin simulation including the different loading directions.

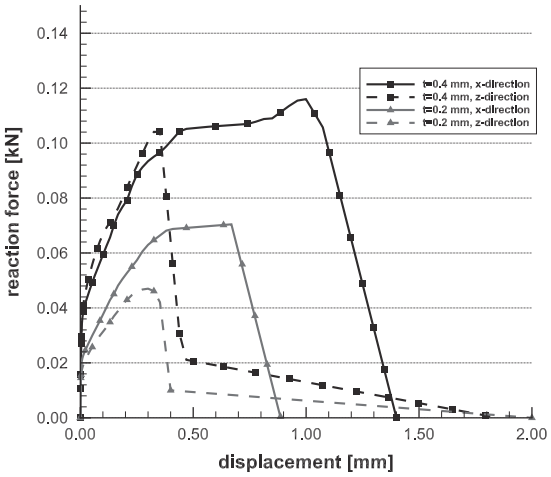

Fig. 12. Load–displacement curves of single-pin simulations.

Fig. 12 exhibits exemplary load–displacement curves in x- and z-direction of two different pin geometries, which differ in the pin thicknesses of $t = 0.2$ mm and $t = 0.4$ mm, respectively.

The differing curve progressions indicate completely different failure mechanisms of the mechanical characteristics caused by shear (x) and normal load (z). The shear loading condition resulted in a visible plastic deformation of the metallic reinforcement especially in the bending radius, which leads to a shearing off of the pin in this region, cf. Fig. 13(a). The configuration of a sheet thickness of $t = 0.4$ mm reaches a maximal load of $f_{pin,x} = 0.117$ kN and the one containing a thickness of $t = 0.2$ mm one of $f_{pin,x} = 0.068$ kN, which implies a reduction of 42%. This reflects also the assumption resulting from the moment of inertia around the y-axis $W_y = (t \cdot w^2)/6$ as described by Großet al. [31], which predicts a linear dependence of the structural mechanics from this parameter. The load–displacement curves of a pin motion along the z-direction showed entirely different characteristics. A similar behavior was described in an Airbus research work [32] discussing experimental pull-out tests, too. A linear-elastic behavior was followed by an abrupt decrease of the reaction load. Subsequently, a further reduction of the reaction force was observed until a displacement of about $\Delta z = 2$ mm, which means a complete pull-out of the reinforcement from the composite material, cf. Fig. 13(b).

The progress of the load–displacement curve was supposed to be the result from a fracture of the bonding surface, which leads to the abrupt decrease of the reaction force. The following smooth decline was assumed to be caused by the friction between the pin and the composite material during the pull-out. The configuration with a pin thickness of $t = 0.4$ mm could be loaded up to $f_{pin,z} = 0.105$ kN and the one with a thickness of $t = 0.2$ mm to $f_{pin,z} = 0.052$ kN, which is equal to a difference of 50%. This emphasizes, that the structural mechanics of this failure mode are not just predicated on the bonding surface between pin and composite, as this was just reduced by 20%. Additional effects as e.g. the bending up of the radius of the pin have to be taken into account. The behavior based on these load–displacement curves was applied for each loading mode to the connector elements by an elastic part followed by a table input to reproduce the nonlinear behavior. The degradation was realized by table input, which was coupled to a damage variable allowing the analysis of the failure mode of each reinforcement.

4.5. Validation of the simplified FE model

The outcome of the simplified implementation method was validated against experimental results. Therefore, among others two single-lap shear geometries according to ASTM 5868 standard [19] were used for the comparison, which featured metal inserts containing a 5×6 and a 4×5 pin configuration (Fig. 14(a) and (b)). All reinforcing elements were built by a thickness of $t = 0.4$ mm, a width of $w = 0.6$ mm and a length of $l = 1.8$ mm. The evaluation was carried out considering the reaction force f

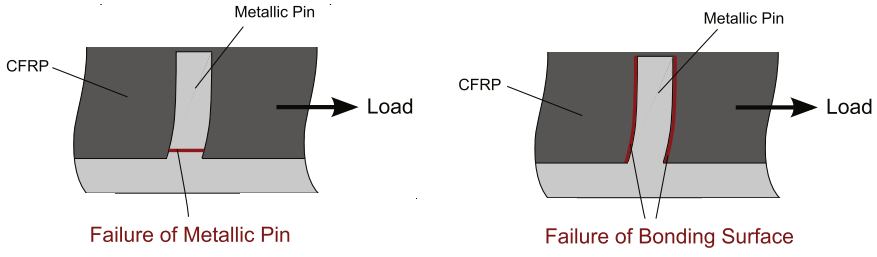

(a) Fracture by shearing off (b) Failure by pull-out

Fig. 13. Failure modes of the reinforcements according to the load case.

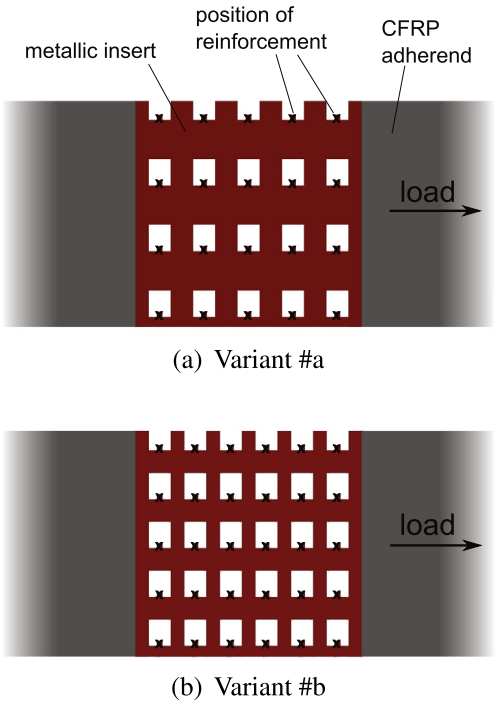

Fig. 14. Geometries of the reinforcement sheets used for the validation of the finite element model.

and the elongation e measured by a 50 mm extensometer around the joint. The resulting load–displacement curves of experiment and simulation of variant #a are opposed in Fig. 15.

Additionally, the output of the finite element model of a co-bonded CFRP–CFRP single-lap shear test without reinforcements, which functions as reference, is presented. This reached an applicable load of $f = 7000$ N and a maximum elongation of $e = 0.085$ mm. The reinforced variant exceeded the load level as well as the elongation obviously. Furthermore, it was observed, that the reinforcement leads to a reduction of the initial stiffness of the joint, which can be ascribed to the deflection of fibers around the reinforcements within the composite adherends. Considering the comparison of experimental and numerical results, the FE model matched the initial stiffness of the joint, which is mostly influenced by the composite adherends. The initial point of failure

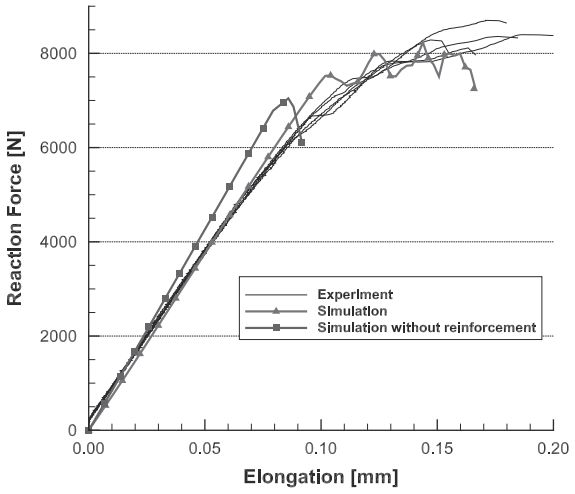

Fig. 15. Numerical and experimental load–elongation curves of variant #a reinforced single-lap shear test specimens.

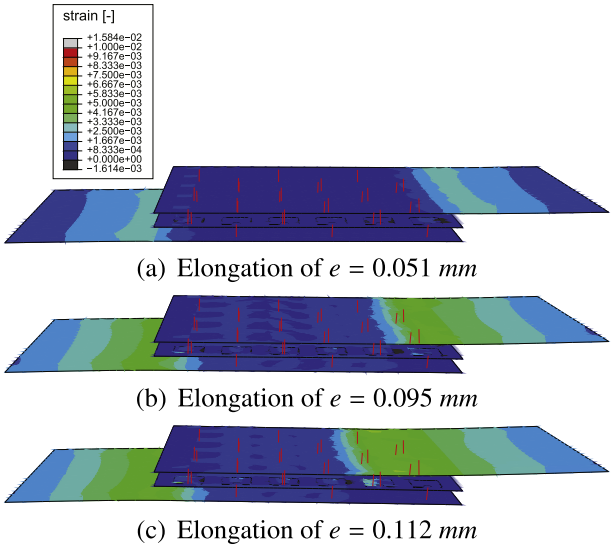

Fig. 16. Strain distribution of single-lap shear test specimen.

at about $f \approx 7000$ N was successfully calibrated using the techniques shown by Lang et al. [4]. The causative failure of the bonding surface is emphasized by Fig. 16(b) including the strain distribution at an elongation of $e = 0.095$ mm. It shows, that the originally symmetrical distribution in Fig. 16(a) changed. The comparison to the unreinforced specimen highlights the increase of damage tolerance by the plastic deformation capability resulting from the reinforcements.

The overall characteristic structural mechanics were captured by the numerical implementation as well as the load level and the length variation of the joining area. The numerical results show a more chattering development of the deformation, which was set into accordance of the failure of rows of the reinforcing elements. Fig. 16(c) including the strain distribution at an elongation of $e = 0.112$ mm underlines this estimation. It states a further development of the asymmetry of the strain distribution. Additionally, the first row of pins within the fractured interface has already failed and the second one is highly loaded showing a minor deformation.

The analysis of the damage variables showed, that the failure of the reinforcements were mainly induced by pulling-out the pins from the composite material. The final fracture of the joint was observed at an elongation of $e = 0.156$ mm concerning the calculated result in contrast to the mean value of the experimentally determined ($e = 0.161$ mm).

Jürgens et al. investigated the structural mechanics of the same configuration with experimental tests [33]. It showed a failure on mainly one side of the reinforcement sheet as the simulation did. Furthermore the experimental results confirmed the failure modes of dominating pin pull-outs from the composite material.

Summarizing the structural performance of the reinforced joint could be captured by the implemented finite element model in an adequate precision.

The comparison of experimental test data and the numerical solution of test specimen with a reinforcement according to variant #b is included in Fig. 17. In contrast to the structural behavior of the unreinforced specimen variant #b showed an improved performance considering the elongation e. Due to the narrowed quantity of reinforcing elements, an increase of the applicable load f could not be declared. Furthermore, the pin reduction entailed a minor discrepancy between the initial stiffness of reinforced and unreinforced specimen in contrast to variant #a. The initial stiffness of the reinforced joint was matched by the numerical modeling. The

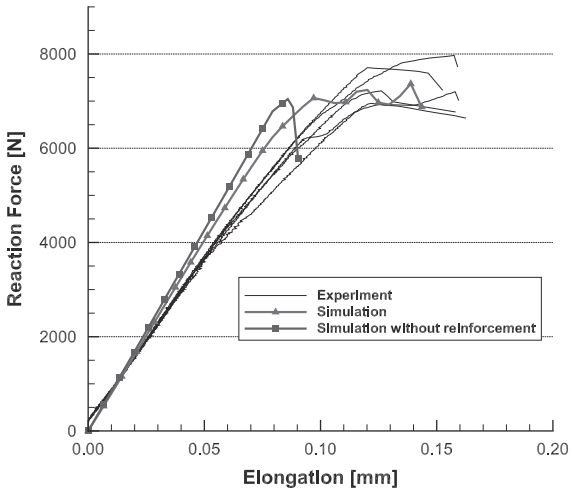

Fig. 17. Numerical and experimental load–elongation curves of variant #b reinforced single-lap shear test specimens.

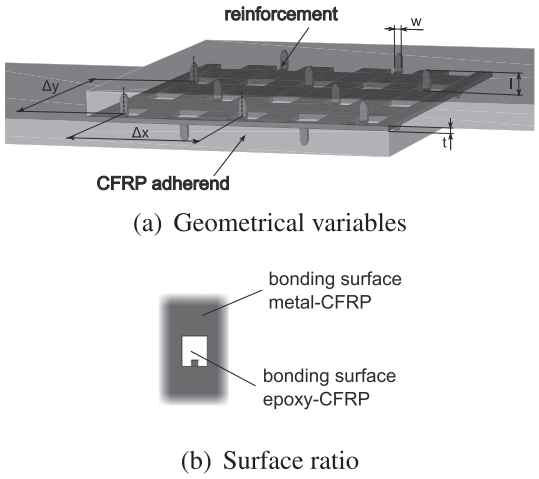

Fig. 18. Design factors analyzed within the variable search.

nonlinear behavior of the experimental data beginning at a load of $f \approx 4200$ N could not be captured by the FE model. The reason of the nonlinearity was assumed to be a manufacturing imperfection of the experimental text specimens in terms of an initial crack at the edge, which was not included in the numerical implementation. Though, the effect of the experiments could be reproduced by eliminating the adhesive in the edges of the reinforced joints imitating an initial crack between the metal sheet and the composite adherend. The experimental results show an initial failure of the bonding surface at approximately $f \approx 7200$ N, which was also matched by the numerical implementation. Taking into account this manufacturing issue and its consequences on the curves, the characteristics resulting from the reinforcements are captured with sufficient accuracy. The maximum applicable load is situated within the experimental data as well as the overall characteristics of the decreasing load level following the initial failure. The ultimate elongation was in comparison to the experimental data estimated too low. In regard to the premature failure of the adhesive bonding of the tests, which lead to a shifting of the curve progression, the elongation caused by the pin reinforcement is nearly equal to the experiments. As the two exemplary configurations showed, the developed modeling technique was able to reproduce the structural characteristics resulting from the metallic reinforcements in an adequate way.

5. Evaluation of the effects resulting from the design factors

The implementation method shown above was used to identify the most influencing design parameters of the reinforcing technique concerning the elongation at failure e as well as the applicable load f at this point. The analyzed factors are illustrated in Fig. 18 including geometrical properties of the reinforcing elements as well as their positioning. Additionally, the ratio of the two implemented cohesive zones concerning the metallic fillets of the metal insert and the epoxy filled areas $\beta = (surface_{metal-CFRP})/(surface_{epoxy-CFRP})$ was taken into account.

The employed approach was aligned to the variable search technique proposed by Shainin [5,6]. For each design variable two levels were defined, which were assigned a negative (−) and positive (+) effect on the objectives. The precise levels of the regarded variables are specified in Table 2. Most of them derived from manufacturing boundaries.

Table 3 summarizes all the trials # with the regarding combinations of the factor levels, which were realized with a numerical implementation. Variants #1 and #2 represent the references with all factors at level (+) or (−), respectively. The remaining variation pairs from #3 and #4 to #13 and #14 include the configurations of the references with just the specific variable, which is analyzed, changed to the contrary level, which allows a detailed evaluation of the influence of the particular factor on the analyzed objectives.

Table 2
Levels of design factors used for the variable search.

Variable		(−)	(+)
Pin/sheet thickness t	[mm]	0.2	0.4
Pin length l	[mm]	1.4	1.8
Pin width w	[mm]	0.46	0.6
Ratio of adhesive surfaces β	[−]	3.5	2.0
Pin distance Δx	[mm]	5.0	4.0
Pin distance Δy	[mm]	7.4	5.5

Fig. 19 includes the chart containing the reaction forces at the point of final failure of configurations #1 to #14. The combination of all positive levels within trial #1 achieved a maximum force of $f = 8.35$ kN. The lowest applicable force $f = 5.80$ kN was reached by the negative reference #2. As assumed, variants #3 to #14 exhibit values between those extreme values. The trials referring to the factors pin/sheet thickness t (#3 and #4), surface ratio β (#9 and #10) and the distance in y-direction Δy (#13 and #14) show the most distinctive deviations from the referential configurations, which suggests a corresponding influence of these parameters. The unequal impact of the level change depending on the positive or negative baseline observed at t and Δy indicates the presence of interdependencies of these factors with other variables.

The dimensionless influences I of each specific variable X on the reaction force f were defined using Eq. (2), compare [34]. The effect was calculated by subtracting the mean reaction force originated from all trials containing the factor X at the (−) level from the mean force resulting from all configurations with variable X at level (+). The factor n is representing the number of analyzed pairs ($n = 7$), which included the referential variants #1 and #2, too:

$$I_{f(X)} = \frac{1}{n}\sum_{i=1}^{n} f(X_{i,pos}) - \frac{1}{n}\sum_{i=1}^{n} f(X_{i,neg}) \tag{2}$$

The chart of the main effects concerning the reaction force f is comprised in Fig. 20. It mirrors the findings regarding the importance of the sheet and pin thickness t as well as the surface ratio β and the distance Δy, all featuring an influence effect $I_f > 1.0$. The importance of the thickness t can be ascribed to the effect on

Table 3
Combinations of the design factors numerically analyzed.

#	t [mm]	l [mm]	w [mm]	β [−]	Δx [mm]	Δy [mm]
1	0.4	1.8	0.6	2.0	4.0	5.5
2	0.2	1.4	0.46	3.5	5.0	7.4
3	0.2	1.8	0.6	2.0	4.0	5.5
4	0.4	1.4	0.46	3.5	5.0	7.4
5	0.4	1.4	0.6	2.0	4.0	5.5
6	0.2	1.8	0.46	3.5	5.0	7.4
7	0.4	1.8	0.46	2.0	4.0	5.5
8	0.2	1.4	0.6	3.5	5.0	7.4
9	0.4	1.8	0.6	3.5	4.0	5.5
10	0.2	1.4	0.46	2.0	5.0	7.4
11	0.4	1.8	0.6	2.0	5.0	5.5
12	0.2	1.4	0.46	3.5	4.0	7.4
13	0.4	1.8	0.6	2.0	4.0	7.4
14	0.2	1.4	0.46	3.5	5.0	5.5

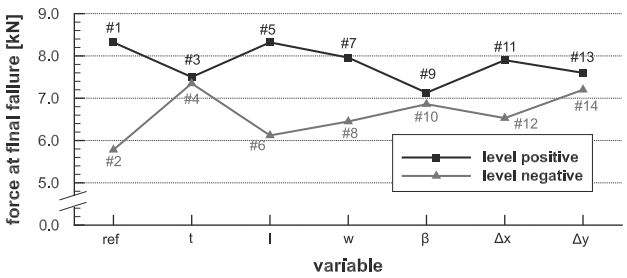

Fig. 19. Reaction forces of the analyzed configurations at the point of final failure.

the resistance of the reinforcing elements. The surface ratio β represents the bonding characteristics considering the reduced bonding quality between metal and composite compared to straight bonding of two composite parts.

It is also obvious, that the density of the reinforcing elements represented by the distances Δx and Δy showed a clear effect on the structural mechanics, though the two directions have to be differentiated. It shows, that the distribution of the pin elements in y-direction implicates an influence, which exceeds the corresponding effect of the density in x-direction by 37%. Due to manufacturing limitations, different levels of these two directions had to be taken into account. Though it was assumed, that a difference of minor 10% of the ratios however does not result in such a difference in the influence on the structural mechanics. The importance of the density in y-direction corresponds to the fact, that the reinforcement in areas of the joint, which are loaded the most, stop the crack from propagating at the beginning. This leads to a higher applicable load.

The geometrical properties of the reinforcing elements themselves of length l and width w were identified as subordinate factors with effects of $I_f \ll 1.0$. For a further investigation of the interactions between the different factors, the interdependencies between the identified main effects were evaluated (Eq. (3)). Though, corresponding combinations between two factors X and Y were analyzed by a subtraction of the mean value of the trials containing both analyzed factors at different levels from the relating mean forces of configurations including all variants at level (+) or (−).

$$I_{f(X,Y)} = \frac{1}{2m}\sum_{i=1}^{m} f(X_{i,pos}, Y_{i,pos}) + \frac{1}{2m}\sum_{i=1}^{m} f(X_{i,neg}, Y_{i,neg}) - \frac{1}{2p}\sum_{i=1}^{p} f(X_{i,pos}, Y_{i,neg}) - \frac{1}{2p}\sum_{i=1}^{p} f(X_{i,neg}, Y_{i,pos}) \tag{3}$$

m and p comply the quantity of the occurring combinations ($m = 5$ and $p = n - m = 2$). The graphical evaluation of this calculation is included in Fig. 21.

It confirms the assumption of significant forms of the interdependency between the thickness t and the distance Δy with an influence of $I_{t*\Delta y} = -0.55$. This value mirrors the statements from above, that a dense reinforcement especially in the run-out areas was seen as influential concerning the applicable load f, which includes a dependency of the distribution as well as the thickness of the used reinforcing geometries. Additionally, the negative algebraic sign indicates a weakening of the objective by a combination of these two factors. Furthermore, interactions $t * \Delta x$, $\beta * \Delta x$ as well as $\Delta x * \Delta y$ are existent, but not that significant. The interaction between the density in the different directions was supposed to be influenced at a certain part by the differences in the levels assigned. The interdependency between the most important factors t and β is not remarkable with a value of $I_{t*\beta} \approx 0$ (see Fig. 21).

Fig. 22 summarizes the results of trials #1 to #14 concerning the elongation at failure e. By the *positive* reference configuration #1, a maximum elongation of $e = 0.154$ mm was achieved. The most *negative* composition #2 lead to a maximum elongation of $e = 0.133$ mm. In contrast to the applicable load f, the proportional difference between these extreme values, which was influenced by the design variables, was significantly reduced.

The most significant influences are notable concerning the pin and sheet thickness t, the surface ratio β as well as the distance Δx. In contrast to the results of the reaction force f, the distance in y-direction Δy did not show a distinct impact. Especially regarding the variables t and β, the non-uniform deviations to the negative and positive reference indicate the existence of interactions with other design variables. The main effects concerning the maximum elongation e were determined using Eq. (4).

$$I_{e(X)} = \frac{1}{n}\sum_{i=1}^{n} e(X_{i,pos}) - \frac{1}{n}\sum_{i=1}^{n} e(X_{i,neg}) \tag{4}$$

The resulting plot is illustrated in Fig. 23. Though representing similar tendencies concerning the importance of thickness t and ratio of adhesives β compared to their influence concerning the reaction force f, changes in the remaining parameters are obvious.

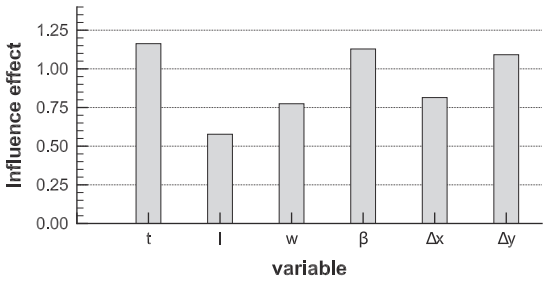

Fig. 20. Main effects of the design variables on the sustainable load.

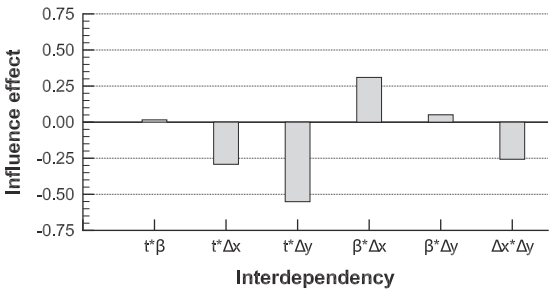

Fig. 21. Dimensionless interdependencies between the most important design variables considering the reaction force of the joint.

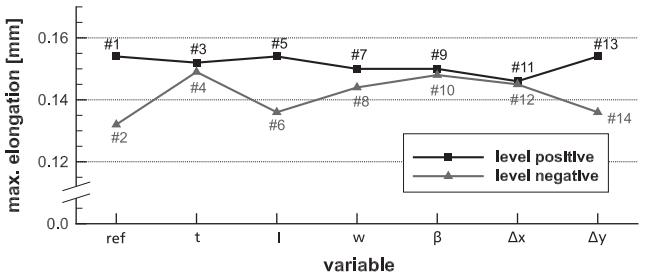

Fig. 22. Maximum elongation of the reinforced joints.

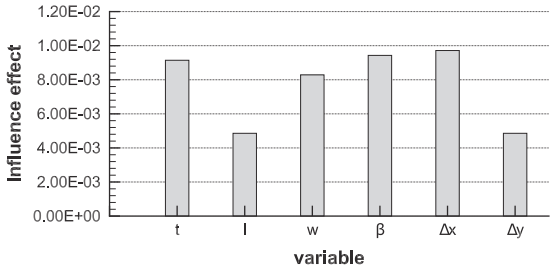

Fig. 23. Main effects of the design variables on the elongation at failure.

Like this, the density in x-direction Δx gained importance. This can be ascribed to the mainly increased density in the central region of the joint, which is reached by the crack at a later point of failure resulting in an enhancement of the damage tolerance. Another factor, which did not show its influence concerning the reaction force, is the width of the pin w. Regarding the elongation e it belongs to the most important design variables. This objective is mainly coupled to the resistance against shear loading within the bonding surface and therefore the moment of inertia around the y-axis of the pin $W_y = (t \cdot w^2)/6$ [31], which underlines the importance of w concerning this type of loading by its quadratic influence. The interdependencies between the most important factors identified in the chart of Fig. 23 were calculated using Eq. (5).

$$I_{e(X,Y)} = \frac{1}{2m}\sum_{i=1}^{m} e(X_{i,pos}, Y_{i,pos}) + \frac{1}{2m}\sum_{i=1}^{m} e(X_{i,neg}, Y_{i,neg}) - \frac{1}{2p}\sum_{i=1}^{p} e(X_{i,pos}, Y_{i,neg}) - \frac{1}{2p}\sum_{i=1}^{p} e(X_{i,neg}, Y_{i,pos}) \tag{5}$$

In analogy to Eq. (3) the subtraction of selected mean values was performed. The evaluated interdependencies are figured in the chart of Fig. 24.

The interdependencies underline the assumption concerning an interaction of the factors t and β with the highest value according to amount of $I_{t*\beta} \approx -0.01$. The interaction $\Delta x * \Delta y$ showed a manifestation comparable to the one considering the reaction force f. Compared to the interdependencies concerning the force f, it is obvious, that most interdependencies hold a negative value. This leads to the fact, that the combination of the respective variables weakens the effect on the elongation e compared to a separate consideration. In summary, the investigation showed, that the two objectives have to be treated separated, as the influences and interactions of the selected variables show a varying performance depending on the objective.

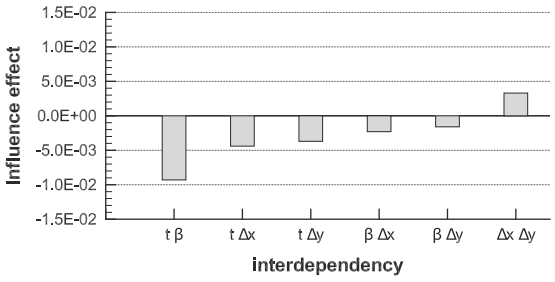

Fig. 24. Interdependencies between the most important design variables considering the elongation at failure.

6. Conclusions

A reinforcing method for bonded composite structures, that is based on the implementation of stamped and three-dimensionally bent metal inlets, was numerically investigated on the example of single-lap shear test specimens. The reinforcing method showed promising results in comparison to referential test specimens considering an improvement of the applicable load level as well as an increase in damage tolerance.

The paper studies the structural behavior of the reinforcing technique on two levels of detail. Based on a detailed implementation, a finite element model on macro-scale was developed to significantly reduce modeling and calculation effort. Both finite element models were successfully validated against experimental test results.

Applying the variable search technique of Shainin, the simplified model was used to identify the factors of the most important main effects considering the objectives of the maximum elongation at failure and the corresponding reaction force. These were identified to the sheet and pin thickness, the design of the stamped areas as well as the distribution of the pins. It showed, that an increase of the pin and sheet thickness leads to an enhanced resistance of the reinforcing elements, which resulted in a significantly raised applicable load as well as damage tolerance of the joint.

Furthermore, the metallic fillets were identified as disturbance factors of the connection resulting from a weakened bonding quality between metal and CFRP compared to areas building a link between two components of the same epoxy based material class. These degraded areas showed their influence both on the damage tolerance and the applicable load.

Additionally, the impact of the distribution of the reinforcing elements was analyzed. This leads to the result, that a higher number of reinforcements perpendicular to the loading direction, which is going along with a strengthening of the most loaded areas of the overlap, mostly affects the applicable load. In contrast to this, a raised density of pins in loading direction, which means an increase of the reinforcing density mainly in the center of the overlapping area, is able to enhance the maximum elongation including the damage tolerance.

Furthermore, the interdependencies between several design parameters could be identified and their characteristics quantified, which showed a different behavior regarding the two objectives. The most important one regarding the applicable load is seen in the interdependency considering the pin/sheet thickness and the density of the reinforcements orthogonal to the loading direction regarding the applicable load. As the interdependency holds a negative value, it indicates, that the combination of these possibilities of enhancing the reinforcement is not able to reach the same improvement as it is assumed considering the potentials of the factors evaluated separately. This characteristic was observed by a majority of the interdependencies considering the elongation at failure. This can be seen as an evidence, that an increase of the reinforcement density leads to a saturation at a certain point.

Acknowledgements

The authors would like to thank the Federal Ministry of Education and Research, Germany, (BMBF) for funding this research within the TransHybrid project.

References

[1] Camanho PP, Hallet S. Composite Joints and Connections: Principles, Modelling and Testing. Woodhead Publishing; 2011.
[2] Grüber B, Hufenbach W, Kroll L, Lepper M, Zhou B. Stress concentration analysis of fibre-reinforced multilayered composites with pin-loaded holes. Compos Sci Technol 2007;67:1439–50.
[3] Nogueira AC, Drechsler K, Hombergsmeier E, Pacchione M. Investigation of the properties and failure mechanism of a damage tolerant 3d-reinforced joint for lightweight structures. In: Proceedings of 6th international technical conference (SETEC), Leiden, Netherlands; 2011.
[4] Lang H, Nogueira AC, Drechsler K, Hombergsmeier E. Development and optimization of an innovative joining technique for composite structures using the finite element method. In: Proceedings of european congress on computational methods in applied sciences and engineering (ECCOMAS 2012), Vienna, Austria; 2012.
[5] Shainin D. Better than taguchi orthogonal tables. In: Proceedings of ASQC quality congress transactions, Anaheim, USA; 1986.
[6] Shainin D, Shainin P. Better than taguchi orthogonal tables. Qual Reliab Eng Int 1988;4:143–9.
[7] Tao Y, Jiao G, Wang B, Chang Y. Effect of *z*-pin's diameter, spacing and overlap length on connecting performance of cmc single-lap joint. Acta Mech Solida Sin 2008:21.
[8] Mouritz A. Compression properties of *z*-pinned composite laminates. Compos Sci Technol 2007;67:3110–20.
[9] Rugg K, Cox B, Massabo R. Mixed mode delamination of polymer composite laminates reinforced through the thickness by z-fibers. Compos A: Appl Sci Manuf 2002;33:177–90.
[10] Byrd L, Birman V. Effectiveness of z-pins in preventing delamination of co-cured composite joints on the example of a double cantilever test. Compos B: Eng 2006;37:365–78.
[11] Kolesnikov B, Herbeck L, Fink A. Fortschrittliche Verbindungstechniken von Faserverbundstrukturen. In: Tagungsband des Deutschen Luft-und Raumfahrtkongresses (DGLR); 2009.
[12] Karpov Y. Joining of high-loaded composite structural components. part 1: design and engineering solutions and performance assessment. Strength Mater. 2006:38.
[13] Son H, Park Y, Kweon J, Choi J. Fatigue behaviour of metal pin-reinforced composite single-lap shear joints in a hygrothermal environment. Compos Struct 2014;108:151–60.
[14] Ucsnik S, Scherer M, Zaremba S, Pahr D. Experimental investigation of a novel hybrid metal-composite joining technology. Compos A: Appl Sci Manuf 2010;41:369–74.
[15] Ucsnik S, Staffenberger S. Numerical model of a cylinder pin reinforced metal to composite single-lap shear joint. In: Proceedings of european congress on computational methods in applied sciences and engineering (ECCOMAS 2012), Vienna, Austria; 2012.
[16] Bianchi F. Numerical modeling of through-thickness reinforced joints, PhD thesis, Cranfield university, School of Engineering; 2012.
[17] Groze F, Achimas G, Lazarescu L, Ceclan V. Springback prediction of the v bending process using finite element simulation. In: Proceedings of 7th international multidisciplinary conference, Romania; 2007.
[18] Nogueira AC. Investigation of a damage tolerant joining technology for lightweight structures, PhD thesis, Technische Universität München; 2014.
[19] ASTM International. West Conshohocken, United States, Standard Test Method for Lap Shear Adhesion for Fiber Reinforced Plastic (FRP) Bonding; 2008.
[20] Hexcel. Hexply® M21 product data sheet, Technical report, Hexcel Corporation; 2007.
[21] Ilyas M. Damage modeling of carbon epoxy laminated composites submitted to impact loading, PhD thesis, Institut Supérieur de l'Aéronautique et de l'Espace, Toulouse; 2010.
[22] Dassault Systèmes Simulia, Abaqus User Subroutines Reference Guide; 2014.
[23] Puck A. Festigkeitsanalyse von Faser-Matrix-Laminaten: Modelle für die Praxis, Hanser, Munich, Vienna; 1996.
[24] Deuschle H. 3D Failure Analysis of UD Fibre reinforced composites: puck's theory within FEA, PhD thesis, Institute of Statics and Dynamics of Aerospace Structures, Universtität Stuttgart; 2010.
[25] Puck A, Deuschle H. Progress in the Puck failure theory for fibre reinforced composites: analytical solutions for 3d-stress. Available at: <www.alfredpuck.de>, Seen at: 05/2014.
[26] Joudon V, Portemont G, Lauro F, Bennani B. Experimental procedure to characterize the mode i dynamic fracture toughness of advanced epoxy resins. Eng Fract Mech 2014;126:166–77.
[27] Lang H, Nogueira AC, Hombergsmeier E, Drechsler K. A numerical analysis of an innovative joining technique for composite structures. In: Proceedings of Sampe Europe – 34th international technical conference & forum (SEICO), Paris, France; 2013.
[28] Dassault Systèmes Simulia, Providence, United States, Selecting Material Parameters in Abaqus for Cohesive Elements Defined in Terms of Traction-Separation. Available at: <www.simulia.com>, Seen at: 06/2012.
[29] Turon A, Davila C, Camanho PP, Costa J. An engineering solution for mesh size effects in the simulation of delamination using cohesive zone models. Eng Fract Mech 2007:74.
[30] Yan C, Mai Y-W, Yuan Q, Ye L, Sun J. Effects of substrate materials on fracture toughness measurement in adhesive joints. Int J Mech Sci 2001;43:2091–102.
[31] Gross D, Hauger W, Schröder J, Wall W. Technische Mechanik 1. Springer; 2008.
[32] Airbus Group Innovations, Internal report: pin pull-out tests, Technical report, Airbus Group Innovations; 2015.
[33] Jürgens M, Nogueira AC, Lang H, Hombergsmeier E, Drechsler K. Influence of an optimized 3d-reinforcement layout on the structural mechanics of co-bonded cfrp joints. In: Proceedings of 16th european conference on composite materials (ECCM), Seville, Spain; 2014.
[34] Klein B. Versuchsplanung – DoE: Einführung in die Taguchi/Shainin-Methodik, Oldenbourg Wissenschaftsverlag; 2011.